Nanoscale

PAPER

View Article Online
View Journal | View Issue

Published on 29 December 2014. Downloaded by Vienna University Library on 09/06/2015 15:01:26.

Cite this: *Nanoscale*, 2015, **7**, 3217

Directional self-assembly of permanently magnetised nanocubes in quasi two dimensional layers†

Joe G. Donaldson[a] and Sofia S. Kantorovich*[a,b]

Received 1st December 2014,
Accepted 25th December 2014

DOI: 10.1039/c4nr07101h

www.rsc.org/nanoscale

To design modern materials with a specific response, the consequences of directionally dependent interactions on the self-assembly of constituent nanoparticles need to be properly understood. Directionality arises in the study of anisometric nanoparticles, where geometry has a drastic effect on the properties observed. Given the fact that magnetic interactions are inherently anisotropic, if one constructs these particles from a magnetic medium, an interesting interplay between the two sources of directionality will occur. We have investigated this scenario by exploring systems of dipolar nanocube monolayers. Using an applied analytical approach, in combination with molecular dynamics simulations, we have determined the ground state structures of individual monolayer clusters. Taking inspiration from experiments, two different fixed dipole orientations for the permanent magnetisation of the nanocubes were considered: the first aligned along the [001] crystallographic axis of each cube, and the second along the [111] axis. We discovered that the structure of the ground state is distinctly different for the two systems of permanently magnetised nanocubes; [001] cubes form dipolar chains in the ground state, whereas those with [111] orientation adopt square lattice structures. The discovered configurations in the ground state represent two different structural motifs, as yet unobserved in the ground state of other magnetic nanoparticle systems.

1. Introduction

Nanoscopic magnetic particles are utilised in many modern functional materials that are extremely versatile and often have desirable switchable properties. Understanding and predicting the processes in which these particles assemble enables tailor-made materials to be built from the bottom up. The specific properties of materials can be designed by exploiting the way in which the constituent particles self-organise. These self-assembly mechanisms are effected by numerous internal and external influences. The magnetic character of the particles will effect the microstructure that is formed, while the shape of the assembling units is a competing factor that will also drastically alter the mechanism and resulting outcome of assembly processes.[1,2] External influences will include the thermodynamic conditions and the presence of a magnetic field. All of these variables can be manipulated in tandem to tune the material for a desired response.

Systems of anisometric magnetic nanoparticles are an exciting area of materials research due to combinations of directionally dependent interactions. For instance, it is possible to introduce changes in the anisotropy of the magnetic interaction, exemplified in experiments on magnetically capped colloids and magnetic Janus particles, as well as the predictions of the shifted dipole model.[3–7] An alternative, however, is to introduce a directionally dependent steric interaction resulting from anisometric particles; there are numerous examples of studies on such particles (for instance rods, ellipsoids and peanuts).[8–13] Tierno recently gave a thorough overview of contemporary anisotropic magnetic colloids, highlighting the range of applicability and structural diversity.[14] Here we are concerned with the consequences of the second scenario, whereby the interplay between particle geometry and inherent anisotropy of the magnetic interaction creates interesting pathways for self-assembly to follow. In particular, we shall focus on particles of perhaps the simplest anisometric shape that one could consider: the cube.

The experimental realisation of cubic particles is now readily reproducible, thanks to advances in colloidal synthesis techniques and nanofabrication.[15–20] Depending on the method of synthesis, a large range of particle sizes is accessible, from truly nanoscopic particles on the order of several nanometers up to the micrometer regime. Systems in the micrometer regime benefit from the ability to apply real-space

[a]*Faculty of Physics, University of Vienna, Boltzmanngasse 5, 1090 Vienna, Austria*
[b]*Ural Federal University, Lenin av. 51, Ekaterinburg, 620083, Russia.*
E-mail: sofia.kantorovich@univie.ac.at

†Electronic supplementary information (ESI) available: Full derivation and explanation of the energy of a regular square dipolar nanocube lattice. See DOI: 10.1039/c4nr07101h

Published on 29 December 2014. Downloaded by Vienna University Library on 09/06/2015 15:01:26.

optical imaging techniques to the study of the assembly process.[21] In contrast to spherical magnetic nanoparticle systems, which form chain and ring structures, cubic particles display a preference for ordered arrays of particles.[22,23]

The spontaneous assembly of superlattices occurs frequently in three dimensional experimental systems, typically consisting of iron oxide nanocubes with varying levels of truncation.[24–26] In micron sized systems of hematite cubes, the particles are too heavy to remain suspended in solution, resulting in the formation of interesting body-centred monoclinic sedimentary crystals.[27] However, in a purely two-dimensional example of hematite cube assembly, simple square lattices have also been observed.[28] Cubes synthesised from materials other than traditional ferrous oxides show interesting variations in behaviour. Lead sulphide nanocubes exhibit an effect whereby the superlattice has a characteristic tilt.[29] Nickel platinum alloy nanocubes form monolayers in which particles stand on their vertices, attributed to their magnetic easy axis lying along the [111] crystallographic direction.[18] This is in contrast to cubes of FePt that have a preference for magnetisation along [001].[30] It is evident that the direction of the net magnetic orientation relative to the cube geometry is an important relationship when predicting the structure of observed clusters. For systems of nanocubes at low temperatures, the assembly mechanism drives the particles to adopt structures that reduce the total magnetic moment of clusters by enclosing the magnetic flux. These structures are termed flux-closure rings in solution and flux-polygons in the presence of interactions with a hydrophilic substrate and are considered to be possible candidates for next generation magnetic memory storage.[31,32] Recent advances in electron holography and micro-SQUID techniques have shown an absence of long-range ferromagnetic ordering in magnetic nanomaterials.[33] Magnetic cubes have also been utilised in the formation of other functional colloidal particles, with imbedded cubic patches or hollow cubic cavities.[2,34] These extended functionalisation schemes have been exploited in the study of active colloids.[35]

From the various parameters that can be controlled in systems of nanoparticles, the effect of particle anisometry on system behaviour has been studied most extensively in the simulation and theory of nonmagnetic systems. Simulations of bulk hard cubes and cuboids, based upon a spherical building block model, have hinted at interesting phase behaviour and the possibility of a liquid-crystalline cubatic phase.[36,37] Subsequent studies, encompassing many other hard polyhedral particles, describe the full range of assembled structures stemming solely from the particle shape.[38–43] Additionally, the discovery of vacancy stabilisation mechanisms in hard cube crystals has been reported.[44] The phase behaviour of so-called 'super balls', which nicely mimic the curvature present in experimentally synthesised cubes, has been mapped out as a function of the particle curvature.[45,46]

If we now consider cube systems that are influenced by dipolar interactions, the observed behaviour is in clear contrast to that of dipolar spheres (as one would expect). The bulk behaviour of dipolar nanocubes has been discussed previously by Zhang *et al.*, who report the assembly of nanorings, nanowires and nanosheets in systems with additional attractive interactions between the nanocube faces.[47] Others report the prediction and observation of lattice-like structures in two-dimensional systems under the influence of weak magnetic fields.[28] The effect of induced dipoles on systems of colloidal cubes in an electrostatic context has also been addressed recently. Interesting phase behaviour was reported, including the presence of a chain fluid phase, a hexagonal columnar phase of these chains, and an ordered crystal phase. The predictions compared favourably to the experimental observations also performed.[48] Returning to the context of magnetism, novel helical superstructures of nanocubes have been recently synthesised. The formation of these structures was attributed to the complicated interplay between van der Waals and the dipole interaction, and entropic forces with the coupling of an external field.[49]

In order to predict and tailor the behaviour of nanocubes on the macroscopic scale, one first needs to understand their self-assembly in the absence of thermal fluctuations (*i.e.* low temperature → 0 K). We utilise a model consisting of elements suggested by John *et al.* (coarse-grained cube structure) and Zhang *et al.* (magnetic dipole approximation).[36,47] This model is used as the basis of low temperature molecular dynamics simulations in which we try to elucidate the possible ground state structures. Alongside simulations, we have used analytical theory to predict the energy of candidate structures. In order for analytical calculations to be tractable, we limit the movement of the cubes' centres of mass to two dimensions (*i.e.* a monolayer); rotations in three dimensions, however, remain possible. This scheme is termed quasi two dimensions (Q2D) and suitably mirrors common experimental arrangements. Applying both of these techniques simultaneously, we hope to elucidate the most favourable structures at low temperatures and, subsequently, infer the structural motif that constitutes the ground state configurations of magnetic nanocube systems.

2. Methodology: simulation & theory

2.1. Particle model

In simulation, cubes were treated as monodisperse rigid bodies interacting *via* magnetic and steric potentials only. The magnetic interaction was characterised by the familiar dipolar approximation, where the interaction between particle magnetic moments $\boldsymbol{m}_i$ and $\boldsymbol{m}_j$ has the form,

$$U_{\mathrm{d}}(ij) = \frac{(\boldsymbol{m}_i \cdot \boldsymbol{m}_j)}{r^3} - \frac{3(\boldsymbol{m}_i \cdot \boldsymbol{r}_{ij})(\boldsymbol{m}_j \cdot \boldsymbol{r}_{ij})}{r^5}. \quad (1)$$

The vector $\boldsymbol{r}_{ij} = \boldsymbol{r}_i - \boldsymbol{r}_j$ denotes the displacement vector between particles i and j with corresponding magnitude of $r = |\boldsymbol{r}_{ij}|$. Therefore, our model corresponds to nanocubes with a ferromagnetic core, *i.e.* these cubes are permanently magnetised, and the direction of the dipole moment is fixed relative

 This journal is © The Royal Society of Chemistry 2015

Published on 29 December 2014. Downloaded by Vienna University Library on 09/06/2015 15:01:26.

to the crystallographic axes. The magnetic interaction strength is traditionally characterised for nanoparticles by a dimensionless parameter λ given by,

$$\lambda = \frac{|\boldsymbol{m}|^2}{kTs^3}. \quad (2)$$

It is defined as the energy per particle of two collinear dipoles at close contact (s) normalised relative to thermal energy, kT. Based upon the different preferred magnetisation orientations for cubes found in experiment, two separate systems with fixed dipole orientation were considered: the first along the [001] crystallographic axis and the other along the [111] axis.

All of our simulations were conducted using the simulation package ESPResSo 3.2.0.[50] This allowed us to utilise the available virtual site construction in order to model the rigid-body motion of the cubes.[51] Each individual cube was constructed by arranging virtual particles, acting as spherical building blocks, to form the complete surface area of the cube. A *real* site was positioned at the cube's centre of mass into which the point dipole of each particle was positioned. The virtual sites of each individual particle are fixed relative to the motion of the corresponding *real* site, enabling rigid-body motion to be reproduced.

In principle, one can vary the number of virtual sites per side of a cube in order to tune the coarseness of the cube representation. Therefore, the total number of spheres comprising the surface is given by $6n^2 - 12n + 8$, where n is the number of spheres per cube side. Upon increasing n, the surface roughness will decrease and edge sharpness will increase: in the limit of $n \to \infty$ the particle will tend towards a perfect cube. In a previous implementation of this model by John *et al.* (using $n = 3$), the spherical units were placed at close contact to one another.[36,37] The virtual site construction employed here enables sites to overlap, allowing for the approximation to a cube to be improved. If we denote the total length of a cube as h, and choose to overlap the surface sites by half the diameter of each site, the virtual site diameter will scale as $\sigma_s = 2h/(n+1)$. Evidently, as the value of n increases the computational cost also increases. A good compromise between simulation length and the best possible representation of the cube was found at a value of $n = 5$. The steric interaction is incorporated by applying it at each surface site individually, where a scaling factor is introduced to adjust for the overlaps. The general form is given by the soft sphere (Weeks–Chandler–Anderson) potential,

$$U_s(r_{ij}) = \left\{ \begin{array}{ll} 4\varepsilon\left[\left(\frac{\sigma_s}{r_{ij}}\right)^{12} - \left(\frac{\sigma_s}{r_{ij}}\right)^{6}\right] + \varepsilon, & r_{ij} < 2^{1/6}\sigma_s \\ 0, & r_{ij} \geq 2^{1/6}\sigma_s \end{array} \right\}, \quad (3)$$

where the range parameter σ_s denotes the surface site diameter.[52] An illustration of the specific model used for all simulations is given in Fig. 1.

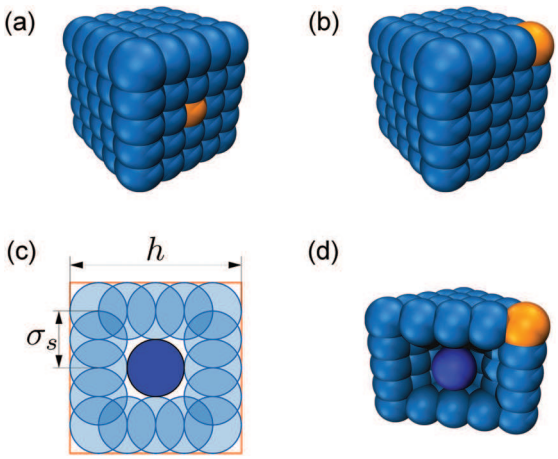

Fig. 1 Visualisations of the cube model used in simulations: (a) Cube particle from simulation where the orange highlight is used to indicate the [001] orientation of the dipole. (b) Cube from simulation with its dipole oriented along [111]. (c) Schematic of a cross-sectional view through the centre of the cube. This view highlights the positioning of the virtual sites at half diameter intervals. A square boarder is drawn (orange) to illustrate the approximation to a perfect cube. The length of the cube is denoted h and the diameter of the constituent spheres by σ_s. (d) Interior of the cubes where the central particle (blue) is now visible.

2.2. Molecular dynamics

Simulations attempting to accurately encapsulate behaviour at low temperatures are notorious for the added subtleties one has to be mindful of. Dipolar systems often have extremely complicated free energy landscapes with many local minima, which represent locally stable structural configurations.[53] It is necessary to ensure that the system does not become trapped in any of these metastable states, which do not represent the true equilibrium energy structure. In order to mitigate this, we have employed canonical Langevin dynamics (LD) simulations allowing for an implicit treatment of the carrier fluid, in combination with the replica-exchange molecular dynamics (REMD) method.[54,55]

During simulations, the particles were confined to a square non-periodic Q2D slab, allowing the magnetic interactions to be dealt with by explicitly summing over particle pairs. A Langevin thermostat was imposed in order to achieve constant-temperature conditions. The one component Langevin equation of motion for a particle i of mass M is given by,

$$M\ddot{x}_i = F_i - \gamma\dot{x}_i + F_{\text{random}}, \quad (4)$$

where F_i is the force on particle i due to the interactions with the other particles, γ is the friction coefficient, and F_{random} is a random Brownian force. The random force is characterised by a gaussian process obeying the fluctuation-dissipation theorem. As such, each component of the force is distributed with a mean of zero and a variance of $\langle {F_{\text{random}}}^2 \rangle = 2\gamma kT$. An equivalent equation of motion is imposed for the rotational degrees of freedom. Given that we are interested in purely equilibrium properties, the dynamical quantities, such as the mass and friction coefficient, are actually physically

Published on 29 December 2014. Downloaded by Vienna University Library on 09/06/2015 15:01:26.

insignificant parameters. Therefore, in simulation their values are set to unity to ensure convenient relaxation to equilibrium. The system was classified in reduced units defined by the cube side length h, the particle mass M and energy parameter ε. The reduced forms of relevant quantities are as follows: length $r^* = r/h$, *i.e.* corresponding to a reduced cube length of $h^* = 1$, magnetic moment $m^{*2} = m^2/h^3\varepsilon$, time $t^* = t(\varepsilon/Mh^2)^{1/2}$ and temperature $T^* = kT/\varepsilon$. The energy parameter ε was chosen in a manner to define a constant magnetic moment of $m^* = 1$. It follows that the λ parameter scales only as $\lambda \propto 1/T^*$. The simulation time-step was set as $\Delta t^* = 0.001$.

The REMD method was used in combination with LD in the following manner. A particular temperature range $\{T_R^*\}$ was selected, representing R individual LD simulations (or replicas) at specific temperatures. Temperatures were sampled from an exponential distribution, beginning at a sufficiently high ambient temperature to a target low temperature. A temperature of at least $T^* = 0.001$ was reached for each cluster size. Each replica consisted of an initial random configuration of cubic particles for the specific cluster size. A single cycle is defined as the propagation of each replica for 1×10^3 time-steps for equilibration, followed by a further 5×10^3 time-steps for data collection. After the completion of each cycle, an attempt was made to exchange configurations between replicas with temperatures adjacent to one another. This exchange is subject to a metropolis criterion; the probability of an exchange between two replicas is $\min(1,\exp[-(1/T_b - 1/T_a)(U_a - U_b)/k])$, where U_x is the total potential energy of configuration x at a temperature T_x. A minimum of 1500 cycles was performed during each simulation. Cluster sizes ranged from 2–25 for the [001] system and 2–16 for [111]. The number of replicas was adjusted accordingly to ensure acceptance ratios were no lower than 20%.

2.3. Theoretical considerations

Throughout our analytical treatment of possible cluster geometries, we assumed perfect cube geometry with a point dipole orientated in either the [001] or [111] directions (see Fig. 2). In order to make analytical predictions of candidate ground state structures tractable, a number of constraints were required. The first was to confine particles to a Q2D layer, which in turn is quite convenient as many experimental systems have this dimensionality. Secondly, calculations were performed on ideal structures with precisely defined geometries, *i.e.* rigid structures based on regular arrays of particles. The methods used here are in line with those applied to spherical particles with and without an external field, as well as to S-D particles, rods and ellipsoids.[6,11,56–58] It should be emphasised that in this work we are considering the zero field regime in both theory and simulation. It is expected that chain and ring structures characteristic of spherical particles will also manifest in systems of nanocubes, albeit in a unique manner.

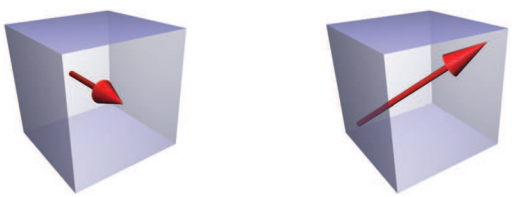

Fig. 2 Theoretical calculations of cluster energies assumed monodisperse perfect cubes as shown. Two systems were considered, one with point dipoles orientated in the [001] crystallographic direction (left hand side), the other pointed in the direction of [111] (right hand side).

3. Ground state structure of particle dimers

To begin, it is useful to consider the energy of configurations of just two dipoles. The lowest energy structures will likely be the basis for clusters of larger numbers of particles. The classic collinear head-to-tail dipole structure (the lowest energy dimer for dipolar spheres) will be used as a point of reference. For spherical particles, the ground state structure can be derived quite intuitively. The effect of the particle geometry is not so intuitively rationalised and, as such, it is useful to explore the candidates for cube dimers in more detail. In order to determine their energies, consider the coordinate system given in Fig. 3(a), shown for [111] but equally applicable to [001]. The dipole of the first particle is localised at the origin, resulting in the following dipolar interaction,

$$U_d(1,2) = -\frac{|\boldsymbol{m}|^2}{|\boldsymbol{r}_{12}|^3}[3\cos\theta(\sin\omega\ \sin\theta\ \cos(\phi-\psi)+\cos\theta\ \cos\omega)]. \quad (5)$$

The angles (θ,φ) define the orientation of the displacement vector and (ω,ψ) define the relative orientation of the second dipole.

When determining the low energy configuration, a sensible approach is to place the cubes at the closest possible contact in order to reduce the distance between dipoles. From here, all

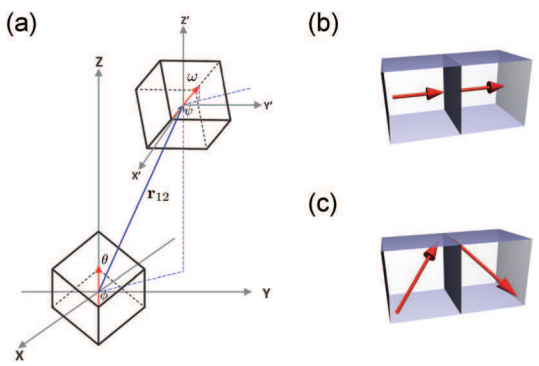

Fig. 3 Ground state configurations for dipolar cube dimers: (a) Coordinate system used for the determination of the dimer energies, shown for [111] but applicable for [001]. The displacement of the second dipole is given by coordinates (r,θ,φ) and its orientation by (ω,ψ). (b) Predicted ground state structure of a [001] dimer, a collinear head-to-tail arrangement. (c) Predicted ground state structure of a [111] dimer; the head-to-tail structure has adopted a zig-zag pattern.

 This journal is © The Royal Society of Chemistry 2015

Published on 29 December 2014. Downloaded by Vienna University Library on 09/06/2015 15:01:26.

the energies of the possible mutual orientations can be calculated. For the lowest energy dimer, consider localising the second dipole on the z-axis ($\theta = \varphi = 0$). We can place this dipole parallel to the z-axis ($\omega = 0$) and position the cubes at close contact so that $|\boldsymbol{r}_{12}| = h$ and assign $|\boldsymbol{m}| = m$. In this case, $U_d^{[001]}(1,2)$ will reduce to the simple form,

$$U_d^{[001]}(1,2) = -\frac{2m^2}{h^3}\cos\omega. \quad (6)$$

The minimum occurs for $\omega = 0$, resulting in a collinear head-to tail configuration. This configuration is the lowest energy for the [001] orientation. Therefore, the dipolar configuration of this dimer is exactly equivalent to the collinear reference. The energy of the structure is $U_d^{[001]}(1,2) = -2m^2/h^3$: when followed with appropriate normalisation by $[m^2/h^3]$ this yields $u_d^{[001]}(1,2) = -2$. A schematic of this lowest energy dimer is given in Fig. 3(b).

The situation for the second orientation is one in which an intuitive answer is not possible. Once again if we consider placing the second cube at the point of closest contact, the lowest energy configuration will be found. For the cube geometry this is, as before, a face-to-face contact. The second dipole is positioned at coordinates $(r,\theta,\phi) = (h, \cos^{-1}(\sqrt{3}/3), \tan^{-1}(-\sqrt{3}) = 2\pi/3)$. Consequently, only six mutual orientations of the dipole are accessible at this contact point. The dipole interaction term is as follows,

$$U_d^{[111]}(1,2) = \frac{m^2}{h^3}\sqrt{2}\sin\omega\sin\left(\frac{\pi}{6} - \psi\right). \quad (7)$$

The interaction is minimised by the second dipole oriented at $(\omega,\varphi) = (\pi - \cos^{-1}(-1/3), 2\pi/3)$. This results in a zig-zag head-to-tail configuration, which is the lowest in energy for the [111] orientation. For [111] cubes, the reference collinear structure actually scales with a dipole separation of $\sqrt{3}h$ (space diagonal of the cube), as opposed to simply h. Evidently, the dipole configuration of the dimer does not relate exactly to the reference case, although the dipoles are still aligned head-to-tail. The energy of the structure is $U_d^{[111]}(1,2) = -4m^2/3h^3$, which, followed by normalisation relative to the [111] collinear reference by $\left[m^2/(\sqrt{3}h)^3\right]$, gives $u_d^{[111]}(1,2) = -4\sqrt{3}$. In comparison to [001], where the ground state is equivalent to the collinear form, the [111] ground state dimer is a factor of $2\sqrt{3}$ lower in energy when compared to its collinear reference. A visual representation of this zig-zag dimer structure is given in Fig. 3(c).

A knowledge of how two dipolar cubes combine will assist in predicting and rationalising microstructure comprised of larger numbers of particles.

4. Ground state microstructure in Q2D

In this section the theoretical predictions of cluster energies of ideal structures are presented. Expressions for the energies of clusters are given per particle and are dimensionless (*i.e.* have been normalised by Nm^2/s^3, where s is the appropriate collinear close contact condition, as seen previously in the definition of λ). To reiterate, the treatment is assuming a system of perfect monodisperse dipolar cubes confined to Q2D. The system with dipole orientation [001] ($s = h$) will be treated first, followed by [111] ($s = \sqrt{3}h$).

4.1. Dipole orientation [001]

It has been shown previously that dipolar spheres exhibit a transition from chain to ring ground states occurring at a cluster size of four.[57] For [001] dipolar cubes, by taking inspiration from the spherical case, chain and ring structures were also considered as possible ground state candidates. The idealised chain structure is a rigid linear body with cubes placed at close contact, resulting in a dipolar separation equal to the length of the cube side. (See Fig. 4(a) for an illustration of the configuration.) The expression found for a chain of cubes in this favourable head-to-tail configuration is analogous to that found for other particle geometries.[11,57] The energy of a chain of N cubes is given by,

$$u_{ch}(N) = -\frac{2}{N}\sum_{k=1}^{N-1}\frac{N-k}{k^3}. \quad (8)$$

The energy is built up by the summation of successive neighbour interactions, *i.e.* nearest neighbour then next nearest neighbour and so on. One can consider the behaviour in the limiting cases of small and large numbers of particles. In the limit of large N the following asymptotic form is found,

$$u_{ch}^{a}(N) = -\frac{2}{N}[N\zeta(3) - \zeta(2)], \quad (9)$$

where $\zeta(x)$ denotes the Riemann-zeta function of order $x = 2,3$. This approximation is accurate to 5% even for chains as short

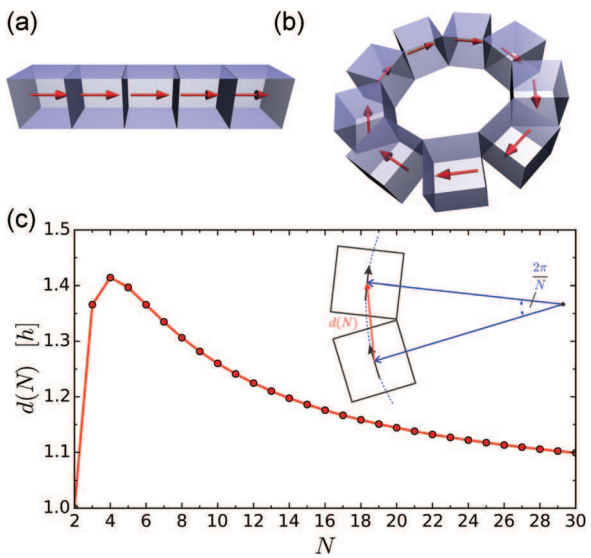

Fig. 4 Candidate ground state structures for [001] dipolar cubes: (a) The rigid linear chain structure with a collinear arrangement of dipoles, example for $N = 5$. (b) Example of ideal ring structure for $N = 9$, where a nonagon is the corresponding polygon. (c) Variation of the nearest neighbour distance $d(N)$ as a function of N. The inset illustrates the location of the distance.

Published on 29 December 2014. Downloaded by Vienna University Library on 09/06/2015 15:01:26.

as four particles. If we only consider interactions between adjacent particles, the following simplification is obtained,

$$u^{n}_{\mathrm{ch}}(N) = -\frac{2(N-1)}{N}. \tag{10}$$

The discrepancy between the full expression and the nearest neighbour limit saturates at approximately 15% as N increases.

The corresponding energy for an ideal ring of dipolar cubes has a more complex form. The term *ideal* refers to the fact that rings are based upon the polygon corresponding to the number of particles in the ring. Another restriction is that dipoles are confined to the two-dimensional plane defined by the ring, and are tangential to its radius at all times. An added complication arises because the distance between neighbouring cubes of the ring (*i.e.* the length of the polygon side) is not constant. In the fortunate situation of an ideal ring of spheres, the nearest neighbour distance for all clusters is equal to the particle diameter. For cubes, this value varies as a function of N. Considering the inset diagram in Fig. 4(c) one can derive a simple expression to describe the variation of the nearest neighbour distance in units of h:

$$d(N) = \left[\cos\left(\frac{\pi}{N}\right) + \sin\left(\frac{\pi}{N}\right)\right]. \tag{11}$$

The plot in Fig. 4(c) shows the variation of this function with increasing N. As N increases, the value of $d(N)$ will tend towards unity because in the limit of infinite N the ring is equivalent to the linear chain. We have verified that the energy of an ideal ring of N cubes is equivalent to that of spheres, provided that the inter-neighbour distance function discussed above is introduced. The full form is as follows,

$$u_{\mathrm{ring}}(N) = \frac{-\sin^3\left(\frac{\pi}{N}\right)}{d(N)^3}\left[\sum_{k=1}^{\left[\frac{N-1}{2}\right]}\frac{\cos^2\left(\frac{\pi k}{N}\right)+1}{\sin^3\left(\frac{\pi k}{N}\right)} + \frac{\mathrm{mod}\,(N+1,2)}{2}\right],$$

where $[(N-1)/2]$ denotes the integer part of $(N-1)/2$ and is present to account for the number of interactions from odd to even membered rings. It is again useful to analyse the behaviour for small and large values of N. For large N one can derive an asymptotic expression of the form,

$$u^{\mathrm{a}}_{\mathrm{ring}}(N) = \frac{-2\zeta(3)}{1+\frac{3\pi}{N}}. \tag{12}$$

This approximation is accurate to within 5% when rings have reached a size of 15 cubes. For small N we consider only the interactions between nearest neighbours; this approximation has the form,

$$u^{n}_{\mathrm{ring}}(N) = \frac{\cos\left(\frac{2\pi}{N}\right) - 3\cos^2\left(\frac{\pi}{N}\right)}{\left[\sin\left(\frac{\pi}{N}\right)+\cos\left(\frac{\pi}{N}\right)\right]^3}. \tag{13}$$

In comparison, with the case of chains, the discrepancy for rings when only nearest neighbour interactions are considered saturates at a higher value of 17%. However, even for small rings this approximation still has an error of just over 10%.

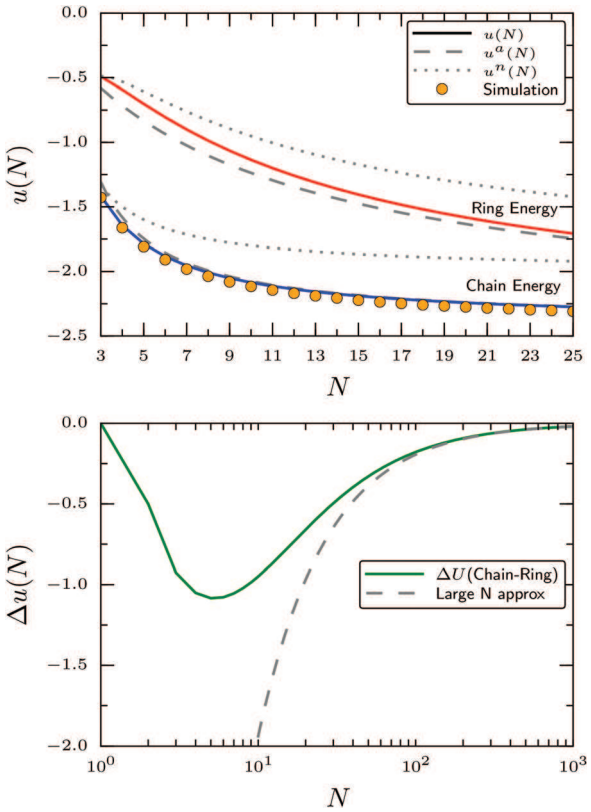

Fig. 5 Energy predictions for the candidate ground state structures: the top plot shows the energy per particle for each cluster type as a function of cluster size. The energies obtained from simulation are given by the orange circles. Shown underneath is the variation of the energy difference between chain and ring structures of equal size.

A comparison of the energy per particle for both cluster types as a function of the size of the cluster is shown at the top of Fig. 5. The approximations for large and small N of each cluster type have also been included for comparison. For each of the cluster sizes considered, the chain configuration is the preferred lowest energy structure. Importantly, no transition of the ground state from one structure to the other is observed. For further clarification, consider the energy trends in the limit of large N, particularly the difference in energy between chains and rings. A further manipulation to eqn (12) is required. As N is large, we can expand the denominator and take the first order correction as follows,

$$u^{\mathrm{a}}_{\mathrm{ring}}(N) = -2\zeta(3)\left(1+\frac{3\pi}{N}\right)^{-1} \approx -2\zeta(3)\left(1-\frac{3\pi}{N}\right). \tag{14}$$

Then, by defining the energy difference between the chain and the ring as $\Delta u^{\mathrm{a}} = u^{\mathrm{a}}_{\mathrm{ch}} - u^{\mathrm{a}}_{\mathrm{ring}}$, we can write,

$$\Delta u^{\mathrm{a}}(N) = \left[-2\zeta(3)+\frac{\pi^2}{3N}\right] - \left[-2\zeta(3)\left(1-\frac{3\pi}{N}\right)\right] = \frac{\pi^2 - 18\pi\zeta(3)}{3N}. \tag{15}$$

 This journal is © The Royal Society of Chemistry 2015

Published on 29 December 2014. Downloaded by Vienna University Library on 09/06/2015 15:01:26.

The second graph of Fig. 5 shows the variation of the energy difference from the full expressions and the approximation above. We can now deduce that $\Delta u^{a} < 0$ even in the limit of infinite N, implying that $u^{a}_{chain} < u^{a}_{ring}$ for all N. Therefore, these idealised chains are still energetically favourable in comparison to rings, regardless of cluster size. Consequently, we predict that chains are the structural motif constituting the ground state configuration of nanocubes with a dipolar orientation of [001].

If we now compare this prediction to the results from simulation, we find evidence to verify these claims. For each of the individually simulated clusters, one finds a preference for the chain structure as predicted. This is confirmed by the excellent agreement between the predicted chain energy and the energy of each cluster from simulation; this data is given in the first plot of Fig. 5 (orange circles). One can also consider a visual identification of clusters through snapshots taken from simulation. A representative selection of cluster sizes was chosen and the corresponding images are given in Fig. 6.

On inspection of the snapshots, it is clear to see that the representation of the cube has a subtle effect on the chain structure. The non-uniform surface structure of the cubes has allowed them to nestle closer together. In terms of magnetic interactions, it is favourable to reduce the distance between dipoles. This is the driving force in the resulting offset between particles as the temperature is decreased. It consequently provides explanation of the slight discrepancy between the predicted and simulated chain energies. The energies from simulation are lower as the cubes have managed to slightly reduce the dipole separation, of which h was assumed in theory. One notices, however, that the variation between simulation and theory stabilises; the effect of the offset diminishes with increasing cluster size. In principle, if one were to increase the model accuracy using the number of spheres per cube side, it would be expected that the size of this offset would decease inline with the sphere diameters. With this in mind, we believe that the good agreement between simulation and theory justifies the use of the composite model, in particular with $n = 5$, as a sensible compromise.

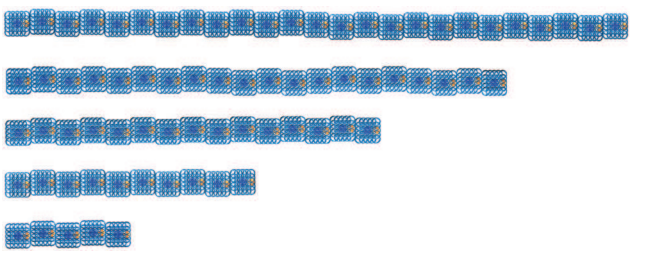

Fig. 6 Simulation snapshot for [001] ground state clusters: series of snapshots for individual cluster sizes N = 5, 10, 15, 20, 25 (from bottom to top). The cubes' surfaces have been made transparent to allow the orientation of dipoles (orange highlight) to be properly seen. The oscillating offset between subsequent cubes can be clearly seen in these images.

From this analysis we conclude that nanocubes with a dipole orientated along the [001] crystallographic axis have a single ground state configuration. In the ground state, regardless of the number of particles, an isolated cluster will adopt the rigid linear chain structure described.

4.2. Dipole orientation [111]

When considering possible candidate ground state structures for [111], an initial approach would be to again postulate structures inspired by the preferences of spherical particles. In this case, however, chains or rings of cubes analogous to those discussed for [001] are higher in energy due to the fact that the inter-dipolar distance now scales with the length of the cube's space diagonal ($\sqrt{3}h$). It follows that candidate structures must complement both the particle geometry and the relative orientation of the dipole within the cubes. An appropriate chain structure to consider would be one based on the configuration of the zig-zag ground state dimer of [111]. A chain of cubes in this favourable zig-zag configuration is depicted in Fig. 7(a). In this chain configuration, an added complication is present as neighbouring dipoles have different orientations. Fortunately the mutual positioning of subsequent dipoles along the chain provides a useful simplification.

To illustrate this, we can look at a simple system of two dipoles confined to a two-dimensional plane. The first dipole occupies the origin and is aligned with the y-axis, $\boldsymbol{m}_1 = |\boldsymbol{m}|(0,1)$. The second dipole is parallel to the first, $\boldsymbol{m}_2 = |\boldsymbol{m}|(0,1)$, but displaced by a vector $\boldsymbol{r}_{12}$, which makes an angle of α with

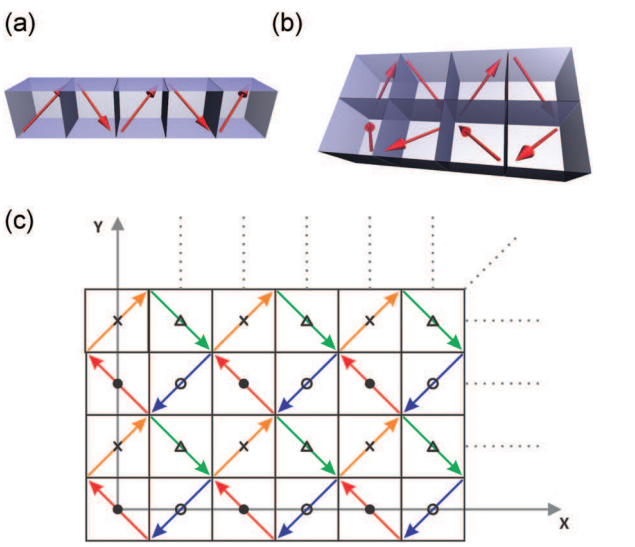

Fig. 7 Candidate ground state structures for [111] dipolar cubes: (a) The rigid chain structure with zig-zag arrangement of dipoles, example for N = 5. (b) Example simple square lattice for N = 8: the construction from ring sub-units is clearly visible. (c) Schematic of the square lattice used for calculations. Dipoles are represented each by a symbol •, ×, Δ and °. By fixing • at the origin, the other dipoles adopt specific positions in the lattice. From here it is possible to visualise the network of interactions between the various dipole combinations.

Published on 29 December 2014. Downloaded by Vienna University Library on 09/06/2015 15:01:26.

the y-axis, $\boldsymbol{r}_{12} = (y\tan\alpha, y)$. The magnitude of this vector is therefore $|\boldsymbol{r}_{12}| = y/\cos\alpha$. The dipolar interaction for the configuration is,

$$U_{\mathrm{d}} = \frac{|\boldsymbol{m}|^2\cos^3\alpha}{y^3} - \frac{3|\boldsymbol{m}|^2 y^2\cos^5\alpha}{y^5}. \tag{16}$$

When the net energy of this interaction is zero, the following relationship holds,

$$U_{\mathrm{d}} = \cos^3\alpha(1 - 3\cos^2\alpha) = 0. \tag{17}$$

This equation has a single physical solution, $\cos\alpha = \sqrt{3}/3$, which corresponds to an angle of $\alpha \approx 54.74°$. The angle α, which measures the orientation between the dipoles and displacement vector, corresponds exactly to the equivalent angle for dipoles over an even number of bonds in the zig-zag chain. Therefore, all of these interactions are zero; only interactions over an odd number of bonds contribute. We know already that nearest neighbour zig-zag dipoles (dimers) have an energy contribution of $-4\sqrt{3}$. To achieve an expression for the zig-zag chain energy, all that is required is a sum of the scaled contributions of the dimer term over an odd number of bonds,

$$u_{\mathrm{zch}}(N) = -\frac{4\sqrt{3}}{N}\sum_{k=0}^{\left[\frac{N-1}{2}\right]}\frac{N-(2k+1)}{(2k+1)^3}. \tag{18}$$

The limit of the sum is again given by $(N-1)/2$ where [...] indicates that only the integer part of the expression is taken; this is to account for odd and even length chains. Once more we can approximate this equation for long chains in the limit of infinite N, and short chains using only nearest neighbour interactions. Each expression is given respectively as,

$$u^{\mathrm{a}}_{\mathrm{zch}}(N) = -\frac{\sqrt{3}}{N}\left[\frac{7}{2}N\zeta(3) - 3\zeta(2)\right], \tag{19}$$

$$u^{n}_{\mathrm{zch}}(N) = -\frac{4\sqrt{3}}{N}(N-1). \tag{20}$$

The asymptote for large N is accurate to within 5% for all chain lengths greater than two. The nearest neighbour approximation has a similar accuracy where the discrepancy saturates rapidly to 5%. The closeness of both approximations can be attributed to the fact that the number of contributing interactions to the energy is significantly reduced with respect to the value of N.

A second structure, which will naturally reflect the intrinsic geometry of the cube and complement the dipole orientation, is a simple square Q2D lattice. The suggested structure of the lattice combines attributes of other structure types. Namely, the lattice can be seen as a regular assembly of alternating zig-zag chains, which in turn form sub-units of four dipoles that adopt deformed ring structures.[28] An illustration of such a lattice is given in Fig. 7(b), where the sub-unit rings are clearly shown.

To calculate the energy of a regular Q2D lattice, with a size of $(n_1 \times n_2)$ cubes, we use the following approach. The dipole at the origin has a fixed orientation of $\frac{|\boldsymbol{m}|}{\sqrt{3}}(-1,1,1)$. It follows, if we define the lattice as an assembly of alternating zig-zag chains, there are a further three possible fixed orientations a dipole can adopt within the lattice. The dipole orientation at each lattice site is now set and can be summarised as follows,

$$\boldsymbol{m}(x,y) = \frac{|\boldsymbol{m}|}{\sqrt{3}}\begin{cases}(-1,1,1) & x,\ y \text{ even or } 0.\\ (1,1,-1) & x \text{ even or } 0; y \text{ odd.}\\ (1,-1,1) & x,\ y \text{ odd.}\\ -(1,1,1) & x \text{ odd}; y \text{ even or } 0.\end{cases} \tag{21}$$

As the dipoles are limited to four orientations within the lattice, there will be a set number of different dipole interactions. The number of interactions, including those between dipoles of the same orientation, is given by the binomial coefficient $\binom{n+r-1}{r}$, with $n = 4$ (number of dipole orientations) and $r = 2$ (pair interactions), which corresponds to 10 possible dipole interactions. To show this, it is useful to consider a representation of the lattice, as in Fig. 7(c), where dipoles are associated with symbols (and colours). By indexing each of the four dipole orientations using the symbols •, ×, Δ and ◦, we can write the energy of the lattice per particle as,

$$\begin{aligned}u_{\mathrm{lat}}(n_1,n_2) = (&u_{\bullet\bullet} + u_{\times\times} + u_{\circ\circ} + u_{\Delta\Delta} + u_{\bullet\times} + u_{\bullet\Delta}\\ &\ldots + u_{\bullet\circ} + u_{\times\Delta} + u_{\times\circ} + u_{\Delta\circ})/(n_1 n_2).\end{aligned} \tag{22}$$

It transpires that the interactions between equivalent dipoles have no net contribution to the lattice energy. That is to say, the sub-lattice of interactions represented by $u_{\bullet\bullet}$, $u_{\times\times}$, $u_{\circ\circ}$ and $u_{\Delta\Delta}$ are individually zero. Thus, the energy per particle as a function of the cluster size ($N = n_1 n_2$) is the sum of the interaction sub-lattices between differing dipoles,

$$u_{\mathrm{lat}}(N) = \frac{1}{N}(u_{\bullet\times} + u_{\bullet\Delta} + u_{\bullet\circ} + u_{\times\Delta} + u_{\times\circ} + u_{\Delta\circ}). \tag{23}$$

Readers who are interested in the form of each of these contributing terms, and an overview of the brute force method used, should consult the accompanying ESI.†

Due to the dipolar configuration within the lattice, its energy is predominantly determined by a relatively small number of interactions terms. As such, we can write a more succinct version of eqn (23) by considering only dominant interaction segments. The most important contribution is from the linear chain segments, in both the vertical and horizontal directions. The expressions account for all successive neighbours in the chain. The second contribution to consider is the net energy of the neighbour interactions along the first order diagonal, *i.e.* dipolar interactions with a separation of $\sqrt{2}h$ only. These diagonal terms have one of two possible energies: favourable, $\varepsilon_{\mathrm{d1}} = -\sqrt{6}/4$ or unfavourable, $\varepsilon_{\mathrm{d2}} = 5\sqrt{6}/4$. The number of each diagonal interaction type needs to be

 This journal is © The Royal Society of Chemistry 2015

Published on 29 December 2014. Downloaded by Vienna University Library on 09/06/2015 15:01:26.

accounted for across the entire lattice. The resulting lattice energy per particle is given as,

$$u^{s}_{\mathrm{lat}}(n_1,n_2) = u_{\mathrm{zch}}(n_2) + u_{\mathrm{zch}}(n_1) + \frac{(n_1-1)(n_2-1)}{N}(\varepsilon_{\mathrm{d1}}+\varepsilon_{\mathrm{d2}}) + \frac{\mathrm{mod}\,[(n_1-1)(n_2-1),2]}{N}(\varepsilon_{\mathrm{d1}}-\varepsilon_{\mathrm{d2}}), \quad (24)$$

where mod[a,b] denotes the residual of the division of a by b. The first two terms account for the vertical and horizontal chains respectively. The final two terms give the contribution from the diagonal interactions, whereby the second performs the required adjustment for lattices of $(n_1 \times n_2) = (2k \times 2k)$ with integer k. This segment expression, in contrast to the general form of eqn (22), allows an asymptote for large lattices to be determined in a straightforward manner. The chain terms are approximated as in eqn (19); in addition, equal populations of both diagonal terms are assumed. The resulting equation is,

$$u^{\mathrm{a}}_{\mathrm{lat}}(n_1,n_2) = u^{\mathrm{a}}_{\mathrm{zch}}(n_2) + u^{\mathrm{a}}_{\mathrm{zch}}(n_1) + \frac{(n_1-1)(n_2-1)}{N}(\varepsilon_{\mathrm{d1}}+\varepsilon_{\mathrm{d2}}). \quad (25)$$

Essentially, the two approximate forms of the lattice energy just described assert that the largest proportion of the lattice energy is determined simply by the number of linear chain segments.

A comparison of the energy per particle as a function of N for the zig-zag chain and the lattice is shown in Fig. 8. The zig-zag chain approximations for large and small N have been included to illustrate their accuracy. The lattice is energetically favourable for each of the cluster sizes considered. Once again, no structural transition of the ground state is observed with increasing N. Energies extracted from simulation support the conclusion that square lattices are formed in the ground state. The simulated energies are found alongside the analytical predictions in Fig. 8 (orange circles). For each individual cluster, there is generally excellent agreement between the predicted and simulated energies. To avoid overcrowding of the main plot, the lattice approximations have been included in the inset of Fig. 8 alongside the same simulation data with which to compare. The segment approximation is remarkably accurate across the entire cluster size range. Obviously for cluster sizes up to $N = 4$, the approximation is in fact exact. However, for larger lattices the energy is overestimated slightly as the destabilising effects of higher order diagonal terms are not accounted for. The large lattice approximation converges quickly to the segment approximation from which it was derived. In turn, for large lattice sizes, the discrepancy to the general form saturates to approximately 9%.

The geometry of each lattice cluster was identified from simulation by studying snapshots of configurations. The ground state structures of individual clusters are those that increase the number of sub-unit rings in the cluster; these can be side-by-side or overlapping. The spectrum of lattice clusters observed for $N = 2$–16 is given in Fig. 9. Panel 4 of Fig. 9 shows the stable ring unit, which acts as the building block of successive clusters. In a larger cluster, its construction is easily observed. For example, in Panel 15, three ring units from Panel 4 have combined, leaving the remaining three particles to position themselves in the top right corner of the cluster, in a manner equivalent to that of Panel 3. A similar procedure is evident in Panel 14; however, due to the fact that there is one less particle, a resulting portion of the structure exhibits a frustration similar to that of the cluster in Panel 6. As such, structural relations between successive clusters depend on the completeness of the constituent rings. In turn, the discontinuous nature of the lattice energy can be attributed to additional particles adopting both favourable and unfavourable arrangements in an effort to form ring structures.

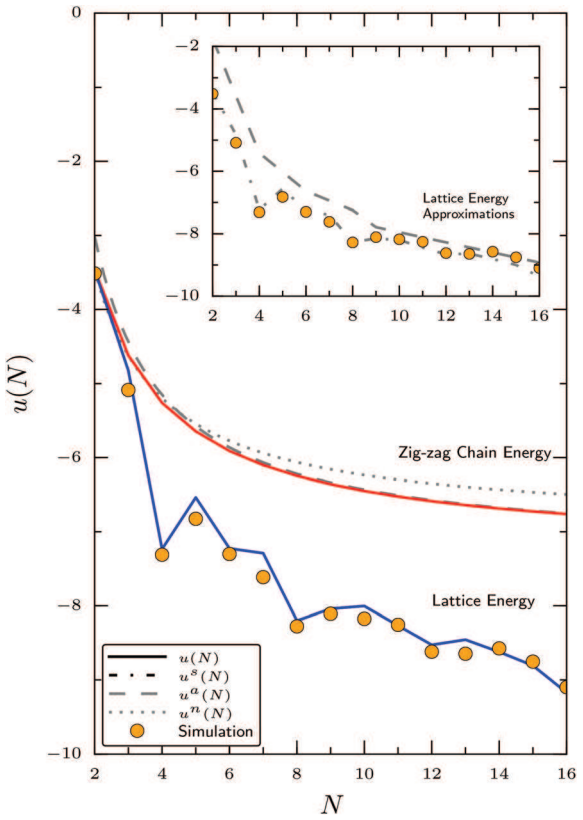

Fig. 8 Energy predictions for [111] candidate ground state structures: The plot shows the predicted energy per particles for each cluster type as a function of cluster size. The energies obtained from simulation are plotted using the orange circles. The approximations for the zig-zag chain are given in the main plot for large N (dashed line) and nearest neighbour interactions only (dotted line). The inset contains the lattice approximations; the segment (dot-dash line) and large N (dashed line).

If one makes a comparison between the configurations and the simulation data, it is clear that rotational freedom in certain cluster sizes alters the total energy. In particular, for $N = 3$, the two non-central nanocubes reduce the cluster energy further by rotating away from full face-to-face contact. The same effect is observed for $N = 5$ where the additional fifth particle, separate from the favourable ring of four, lowers the cluster energy by performing a similar rotation. This added rotation freedom was not accounted for in calculations. As a

Published on 29 December 2014. Downloaded by Vienna University Library on 09/06/2015 15:01:26.

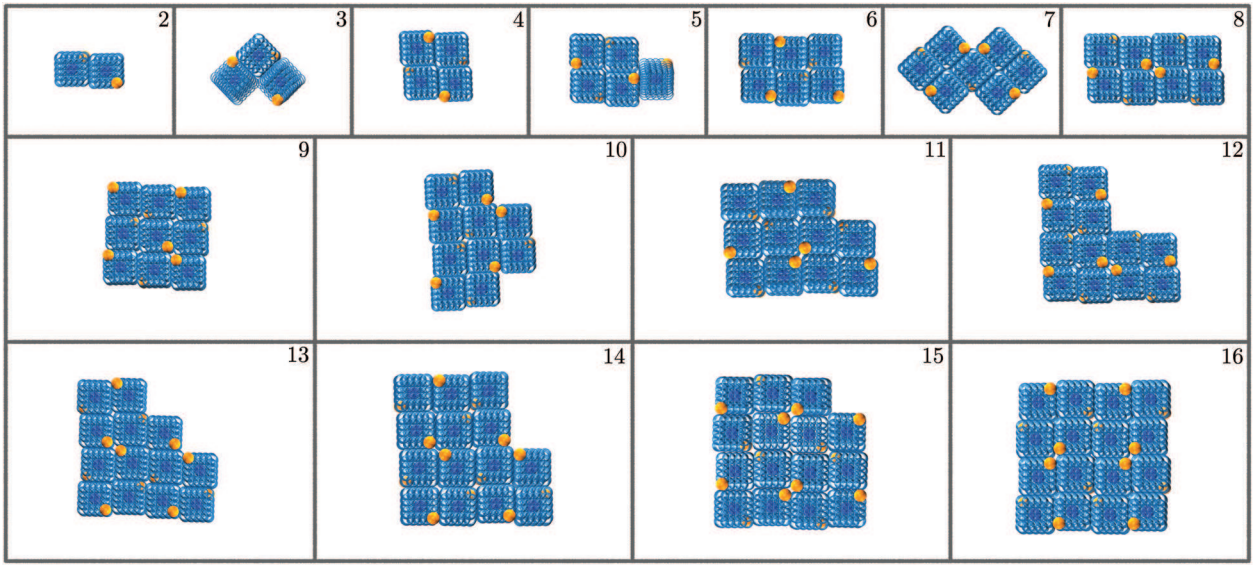

Fig. 9 Simulation snapshots for [111] ground state clusters: snapshot series for individual clusters; the respective size of each is given in the top right hand corner of each Panel. The cubes' surfaces have been made transparent to allow the orientation of dipoles (orange highlights) to be properly seen. The formation of the sub-unit rings is portrayed from cluster to cluster.

result, for clusters where nanocubes are free of confinement by two or more other particles, there are larger deviations from theory. The subtle effect of surface roughness allows cubes to nestle closer to one another. It is clear, however, that the consequences of this artefact are small and the analytical predictions are still valid. One should also note the reduction in the energy fluctuations as the lattice size increases; this is evident in both simulation and theory.

From the evidence we have presented, it is clear that nanocubes with a dipole orientated along the [111] crystallographic axis have a single ground state configuration: a simple square lattice. However, various manifestations of the lattice are found depending on the cluster size. This stems from the creation of favourable four membered rings: the universal motif of the ground state. Dipolar nanocubes of this orientation are the first reported magnetic nanoparticles to form close-packed lattices in isolated ground state clusters. Interestingly, due to the strong energetic favourability of four membered rings, it is foreseeable that the behaviour of a suspension of [111] nanocubes at ambient temperature would be dominated by the formation of $N = 4$ clusters.

4.3. Magnetic character of nanocube clusters

Finally, it is necessary to comment briefly on the magnetic characteristics of the ground state structures that we have found. A simple but useful way of quantifying this is to determine the total magnetic dipole moment of each cluster. The magnitude of the total moment normalised by that of a single particle is given as,

$$D_m(N) = \frac{\sqrt{\left(\sum_{i=1}^{N} {m_x}^i\right)^2 + \left(\sum_{i=1}^{N} {m_y}^i\right)^2 + \left(\sum_{i=1}^{N} {m_z}^i\right)^2}}{|\boldsymbol{m}|}. \qquad (26)$$

The components of the i^{th} dipole of the cluster have been denoted $\boldsymbol{m}_i = ({m_x}^i, {m_y}^i, {m_z}^i)$. D_m describes the individual magnetisation of each cluster relative to that of a single free nano cube.

For the case of [001] nanocubes, given the fact that the ground states are collinear chains, the value of D_m will in theory increase identically with N. Consequently, the value of the total dipole moment per particle, $d_m(N) = D_m/N$, will be a constant equal to unity, as shown in Fig. 10. The agreement between theory and simulation is excellent; the nanocubes in each chain are very precisely oriented in a single direction. The result from this straightforward process has unique significance. To the best of our knowledge, this is the first example of a magnetic nanoparticle system whose configuration, in isolated clusters, does not form to enclose the magnetic flux in

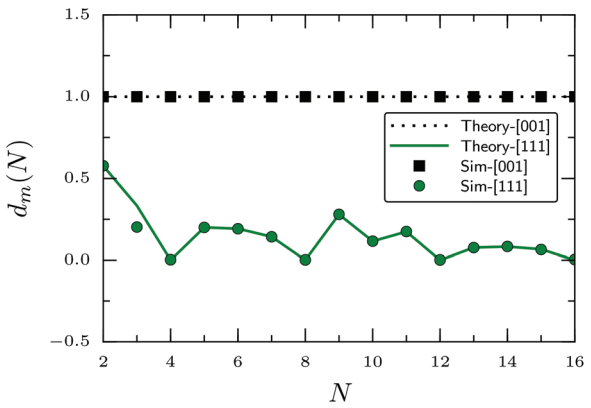

Fig. 10 Variation of total dipole moment for each system as a function of cluster size. Lines are derived from analytical calculation and the points are from simulation. The discrepancy present for $N = 3$ can be attributed to the rotational offset of two of the cluster's particles.

 This journal is © The Royal Society of Chemistry 2015

Published on 29 December 2014. Downloaded by Vienna University Library on 09/06/2015 15:01:26.

Table 1 Summary of the variation of total dipole moment per particle, highlighting the similarities between different cluster sizes

Cluster size/N	Total moment per particle/d_m
4, 8, 12, 16	0
3, 5, 7, 13, 15	$\frac{1}{N}$
2, 6, 10, 14	$\frac{2\sqrt{3}}{3N}$
11	$\frac{\sqrt{11}}{3N}$
9	$\frac{\sqrt{57}}{3N}$

the ground state. The individual structures have a non-zero total dipole moment irrespective of cluster size, which one would expect to result in a strong initial magnetic susceptibility.

In contrast, for [111] nanocubes, the fluctuating cluster energies will give rise to fluctuations in the total magnetic moment. The variation of the total dipole moment per particle, $d_m(N)$, is given in Fig. 10. Despite the fluctuations, trends can be drawn between different clusters (presented in Table 1). Two important observation can be made. First of all, d_m tends to zero with increasing N for each classification. Secondly, clusters where a full complement of rings is formed (*i.e.* clusters where mod[N,4] = 0) have zero total moment as the magnetic flux is completely enclosed. Thus, the system generally behaves in the conventional manner where particles assemble in structures that minimise the magnetic flux in the ground state.

5. Conclusion

The competition between directional interactions offers various pathways for self-assembly, each with exciting possibilities. Here we have discussed the interesting example of dipolar nanocubes. In order to use a combination of analytical theory and molecular dynamics simulations, the nanocubes were confined to a Q2D monolayer. We have studied the behaviour of these magnetic nanocubes in the limit of T = 0 K, with the aim of elucidating the structural traits of isolated ground state clusters. Two orientations of the dipole relative to the cube surface were considered, namely in the crystallographic directions [001] and [111].

For orientation [001], we discovered that linear chain aggregates with a collinear dipolar configuration occupy the ground state. We performed analytical calculations of the chain energy and found consistent agreement with the results of replica exchange molecular dynamics simulations. This expected ground state is the first such example of a magnetic nanoparticle system whose isolated clusters do not exhibit any tendency to enclose the magnetic flux.

In the case of [111] oriented cubes, the ground state was found to consist of structures derived from a simple square lattice. The lattice combines traits of other structure types; it is an antiparallel assembly of zig-zag chains, which in turn form favourable rings of four dipoles. A theoretical framework was developed to determine the energy of these lattice structures and compared favourably to simulations. Again this is a novel system, thanks to the close-packed lattice ground state, a structure not yet observed in other magnetic nanoparticles at 0 K.

From the evidence we have presented here, it is plausible that macroscopic suspension of these nanocubes could exhibit similarly interesting magnetic properties. In order to explore this, we aim to make predictions about the macroscopic magnetic properties of nanocubes by calculating the initial magnetic susceptibility, work that is currently ongoing.

Acknowledgements

The research has been partially supported by Austrian Science Fund (FWF): START-Projekt Y 627-N27, RFBR grant mol-a-ved 12-02-33106, the Ural Federal University stimulating programme and by the Ministry of Education and Science of the Russian Federation (Contract 02.A03.21.000, Project 3.12.2014/K).

References

1 S. C. Glotzer and M. J. Solomon, *Nat. Mater.*, 2007, **6**, 557.
2 S. Sacanna, M. Korpics, K. Rodriguez, L. Coln-Melndez, S.-H. Kim, D. J. Pine and G.-R. Yi, *Nat. Commun.*, 2013, **4**, 1688.
3 L. Baraban, D. Makarov, M. Albrecht, N. Rivier, P. Leiderer and A. Erbe, *Phys. Rev. E: Stat. Phys., Plasmas, Fluids, Relat. Interdiscip. Top.*, 2008, **77**, 031407.
4 S. K. Smoukov, S. Gangwal, M. Marquez and O. D. Velev, *Soft Matter*, 2009, **5**, 1285.
5 K. P. Yuet, D. K. Hwang, R. Haghgooie and P. S. Doyle, *Langmuir*, 2010, **26**, 4281.
6 S. Kantorovich, R. Weeber, J. J. Cerda and C. Holm, *Soft Matter*, 2011, **7**, 5217.
7 A. I. Abrikosov, S. Sacanna, A. P. Philipse and P. Linse, *Soft Matter*, 2013, **9**, 8904.
8 M. Yan, J. Fresnais and J.-F. Berret, *Soft Matter*, 2010, **6**, 1997.
9 A. Günther, P. Bender, A. Tschöpe and R. Birringer, *J. Phys.: Condens. Matter*, 2011, **23**, 325103.
10 P. Tierno, R. Albalat and F. Sagus, *Small*, 2010, **6**, 1749.
11 S. Kantorovich, E. Pyanzina and F. Sciortino, *Soft Matter*, 2013, **9**, 6594.
12 Y. Wang, X. Su, P. Ding, S. Lu and H. Yu, *Langmuir*, 2013, **29**, 11575.
13 S. H. Lee and C. M. Liddell, *Small*, 2009, **5**, 1957.
14 P. Tierno, *Phys. Chem. Chem. Phys.*, 2014, **16**, 23515.
15 Y. Sun and Y. Xia, *Science*, 2002, **298**, 2176.
16 M. V. Kovalenko, M. I. Bodnarchuk, R. T. Lechner, G. Hesser, F. Schäffler and W. Heiss, *J. Am. Chem. Soc.*, 2007, **129**, 6352.
17 S. Sacanna and D. J. Pine, *Curr. Opin. Colloid Interface Sci.*, 2011, **16**, 96.

Published on 29 December 2014. Downloaded by Vienna University Library on 09/06/2015 15:01:26.

18 J. L. Cuya Huaman, S. Fukao, K. Shinoda and B. Jeyadevan, *CrystEngComm*, 2011, **13**, 3364.
19 L. Rossi, S. Sacanna, W. T. M. Irvine, P. M. Chaikin, D. J. Pine and A. P. Philipse, *Soft Matter*, 2011, **7**, 4139.
20 E. Wetterskog, M. Agthe, A. Mayence, J. Grins, D. Wang, S. Rana, A. Ahniyaz, G. Salazar-Alvarez and L. Bergström, *Sci. Technol. Adv. Mater.*, 2014, **15**, 055010.
21 J.-M. Meijer, F. Hagemans, L. Rossi, D. V. Byelov, S. I. Castillo, A. Snigirev, I. Snigireva, A. P. Philipse and A. V. Petukhov, *Langmuir*, 2012, **28**, 7631.
22 K. Butter, P. H. Bomans, P. M. Frederik, G. J. Vroege and A. P. Philipse, *J. Phys.: Condens. Matter*, 2003, **15**, S1451.
23 M. Klokkenburg, R. P. A. Dullens, W. K. Kegel, B. H. Erné and A. P. Philipse, *Phys. Rev. Lett.*, 2006, **96**, 037203.
24 A. Ahniyaz, Y. Sakamoto and L. Bergström, *Proc. Natl. Acad. Sci. U. S. A.*, 2007, **104**, 17570.
25 S. Disch, E. Wetterskog, R. P. Hermann, G. Salazar-Alvarez, P. Busch, T. Brückel, L. Bergström and S. Kamali, *Nano Lett.*, 2011, **11**, 1651.
26 S. Disch, E. Wetterskog, R. P. Hermann, D. Korolkov, P. Busch, P. Boesecke, O. Lyon, U. Vainio, G. Salazar-Alvarez, L. Bergström and T. Brückel, *Nanoscale*, 2013, **5**, 3969.
27 J.-M. Meijer, D. V. Byelov, L. Rossi, A. Snigirev, I. Snigireva, A. P. Philipse and A. V. Petukhov, *Soft Matter*, 2013, **9**, 10729.
28 M. Aoshima, M. Ozaki and A. Satoh, *J. Phys. Chem. C*, 2012, **116**, 17862.
29 Z. Quan, W. Siu Loc, C. Lin, Z. Luo, K. Yang, Y. Wang, H. Wang, Z. Wang and J. Fang, *Nano Lett.*, 2012, **12**, 4409.
30 M. Chen, J. Kim, J. P. Liu, H. Fan and S. Sun, *J. Am. Chem. Soc.*, 2006, **128**, 7132.
31 Y. Xiong, J. Ye, X. Gu and Q.-w. Chen, *J. Phys. Chem. C*, 2007, **111**, 6998.
32 M. W. Szyndler and R. M. Corn, *J. Phys. Chem. Lett.*, 2012, **3**, 2320.
33 B. Faure, E. Wetterskog, K. Gunnarsson, E. Josten, R. P. Hermann, T. Bruckel, J. W. Andreasen, F. Meneau, M. Meyer, A. Lyubartsev, L. Bergström, G. Salazar-Alvarez and P. Svedlindh, *Nanoscale*, 2013, **5**, 953.
34 S. Sacanna, L. Rossi and D. J. Pine, *J. Am. Chem. Soc.*, 2012, **134**, 6112.
35 J. Palacci, S. Sacanna, A. P. Steinberg, D. J. Pine and P. M. Chaikin, *Science*, 2013, **339**, 936.
36 B. S. John, A. Stroock and F. A. Escobedo, *J. Chem. Phys.*, 2004, **120**, 9383.
37 B. S. John and F. A. Escobedo, *J. Phys. Chem. B*, 2005, **109**, 23008.
38 S. Torquato and Y. Jiao, *Nature*, 2009, **460**, 876.
39 U. Agarwal and F. A. Escobedo, *Nat. Mater.*, 2011, **10**, 230.
40 Y. Jiao and S. Torquato, *J. Chem. Phys.*, 2011, **135**, 151101.
41 P. F. Damasceno, M. Engel and S. C. Glotzer, *Science*, 2012, **337**, 453.
42 N. Volkov, A. Lyubartsev and L. Bergström, *Nanoscale*, 2012, **4**, 4765.
43 A. P. Gantapara, J. de Graaf, R. van Roij and M. Dijkstra, *Phys. Rev. Lett.*, 2013, **111**, 015501.
44 F. Smallenburg, L. Filion, M. Marechal and M. Dijkstra, *Proc. Natl. Acad. Sci. U. S. A.*, 2012, **109**, 17728.
45 R. D. Batten, F. H. Stillinger and S. Torquato, *Phys. Rev. E: Stat. Phys., Plasmas, Fluids, Relat. Interdiscip. Top.*, 2010, **81**, 061105.
46 R. Ni, A. P. Gantapara, J. de Graaf, R. van Roij and M. Dijkstra, *Soft Matter*, 2012, **8**, 8826.
47 X. Zhang, Z. Zhang and S. C. Glotzer, *J. Phys. Chem. C*, 2007, **111**, 4132.
48 H. R. Vutukuri, F. Smallenburg, S. Badaire, A. Imhof, M. Dijkstra and A. van Blaaderen, *Soft Matter*, 2014, **10**, 9110.
49 G. Singh, H. Chan, A. Baskin, E. Gelman, N. Repnin, P. Krl and R. Klajn, *Science*, 2014, **345**, 1149.
50 H. J. Limbach, A. Arnold, B. Mann and C. Holm, *Comput. Phys. Commun.*, 2006, **174**, 704.
51 A. Arnold, O. Lenz, S. Kesselheim, R. Weeber, F. Fahrenberger, D. Roehm, P. Koovan and C. Holm, *Mesh-free Methods for Partial Differential Equations VI*, Springer, Berlin Heidelberg, 2013, vol. 89, pp. 1–23.
52 J. D. Weeks, D. Chandler and H. C. Andersen, *J. Chem. Phys.*, 1971, **54**, 5237.
53 J. D. Farrell, C. Lines, J. J. Shepherd, D. Chakrabarti, M. A. Miller and D. J. Wales, *Soft Matter*, 2013, **9**, 5407.
54 P. Allen and D. Tildesley, *Computer simulation of liquids*, Clarendon Press, 1987.
55 Y. Sugita and Y. Okamoto, *Chem. Phys. Lett.*, 1999, **314**, 141.
56 V. Danilov, T. Prokopyeva and S. Kantorovich, *Phys. Rev. E: Stat. Phys., Plasmas, Fluids, Relat. Interdiscip. Top.*, 2012, **86**, 061408.
57 T. A. Prokopieva, V. A. Danilov, S. S. Kantorovich and C. Holm, *Phys. Rev. E: Stat. Phys., Plasmas, Fluids, Relat. Interdiscip. Top.*, 2009, **80**, 031404.
58 R. Weeber, M. Klinkigt, S. Kantorovich and C. Holm, *J. Chem. Phys.*, 2013, **139**, 214901.

 This journal is © The Royal Society of Chemistry 2015